Direct subwavelength imaging and control of near-field localization in individual silver nanocubes

Mårsell, Erik; Svärd, Robin; Miranda, Miguel; Guo, Chen; Harth, Anne; Lorek, Eleonora; Mauritsson, Johan; Arnold, Cord; Xu, Hongxing; L'Huillier, Anne; Mikkelsen, Anders; Losquin, Arthur

Published in:
Applied Physics Letters

DOI:
10.1063/1.4935831

2015

Document Version:
Peer reviewed version (aka post-print)

Direct subwavelength imaging and control of near-field localization in individual silver nanocubes

Erik Mårsell,[1] Robin Svärd,[1] Miguel Miranda,[1] Chen Guo,[1] Anne Harth,[1] Eleonora Lorek,[1] Johan Mauritsson,[1] Cord L. Arnold,[1] Hongxing Xu,[1,2] Anne L'Huillier,[1] Anders Mikkelsen,[1] and Arthur Losquin[1, a)]

[1)] *Lund University, Department of Physics, PO Box 118, 221 00 Lund, Sweden*

[2)] *School of Physics and Technology, and Institute for Advanced Studies, Wuhan University, Wuhan 430072, China*

(Dated: 3 November 2015)

We demonstrate control of near-field localization within individual silver nanocubes through photoemission electron microscopy combined with broadband, few-cycle laser pulses. We find that the near-field is concentrated at the corners of the cubes, and that it can be efficiently localized to different individual corners depending on the polarization of the incoming light. The experimental results are confirmed by finite-difference time-domain simulations, which also provide an intuitive picture of polarization dependent near-field localization in nanocubes.

[a)] Electronic mail: arthur.losquin@fysik.lth.se

The localization of optical near-fields in nanostructures holds great promise for many applications, including sensing[1], nonlinear spectroscopy[2,3], and optoelectronic device technology[4]. Special attention has been focused on the active spatial and temporal control of localized fields induced by femtosecond laser pulses in metallic nanostructures[5,6]. Such control may facilitate ultrafast optical excitation localized on a scale much smaller than the free-space wavelength, or serve as a basis for plasmonic devices[7,8]. However, reaching optimum control of the nanolocalized near-fields requires both well-defined nanostructures and proper characterization methods.

In recent years, metal nanocubes have shown to be especially interesting nanoobjects due to their simple geometry and controlled synthesis in combination with broadband field enhancement, thus offering a playground to investigate various plasmon-related phenomena[3,9–20]. Single-crystalline nanocubes terminated by {100}-type facets can be rationally synthesized using a polyol process[21]. Cubes support a large number of surface plasmon modes with dipolar as well as multipolar character, which enables field enhancement across a wide spectral range[11,13]. However, challenges remain in measuring the local near-field at a subwavelength scale. Previous experimental studies on metal nanocubes have measured various linear[10,13] or nonlinear[3,16] optical properties with a spatial resolution limited by optical diffraction, or studied the surface plasmon modes with high resolution using fast electron based spectroscopies[14,15,19,20]. Near-field imaging was also performed using indirect photochemical methods[17,18]. These studies have concluded that the optical properties and the field enhancement of single nanocubes are strongly dependent on the orientation of the particles with respect to the incident laser polarization[3,16–18]. However, neither of these methods provided a full and direct access to the optically induced near-field within single nanoparticles as a function of laser polarization, which requires both optical excitation and simultaneous spatially resolved detection. Such direct subwavelength imaging of the near-field can be achieved by multiphoton photoemission electron microscopy (PEEM), which uses nonlinearly emitted photoelectrons to form an image of the enhanced near-field with sub-50 nm resolution. During the past decade, PEEM has been used to image localization and control of the near field in various metallic nanostructured samples[22–25]. By further combining PEEM with broadband few-cycle laser pulses[26], strong localized near-fields resulting from broadband field enhancement can be imaged. Such a combination provides a powerful characterization tool towards numerous plasmonic applications, ranging from

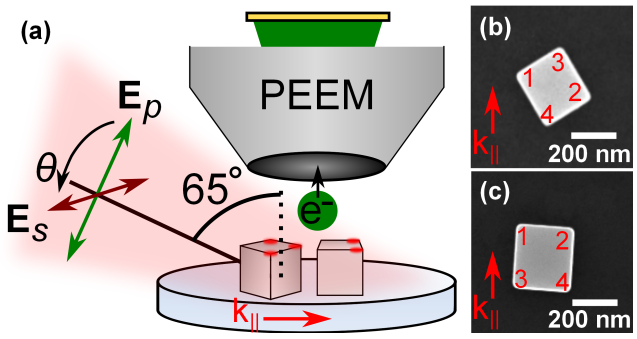

FIG. 1. (a) Side-view schematic of the experiment, including the definition of the polarization angle θ as the deviation (in the clockwise direction as seen in the direction of propagation) from p-polarization. (b–c) SEM images of two silver nanocubes. The nanocubes have approximately the same orientation as in the PEEM images shown in figure 2. $k_{||}$ represents the projection onto the sample plane of the wave vector of the incoming light relative to the nanocubes in the PEEM experiments. For each cube, the corners are labelled from 1 to 4 such that corners 1 and 2 are on opposite sides of the plane of incidence.

ultrafast optics[5,6] to enhancement of solar radiation[27].

In this work, we image the localized near-field in individual silver nanocubes using a photoemission electron microscope together with a broadband laser oscillator delivering few-cycle pulses. We find that the strongest near-fields are localized at the corners of the cubes. The enhanced near-field can further be switched to single corners by adjusting the polarization of the exciting light. The polarization concentrating the photoemission to a specific individual corner is found to be close to when the electric field vector is aligned with the body diagonal passing through that particular corner. The polarization-dependent photoemission distribution is reproduced using finite-difference time-domain (FDTD) simulations.

Silver nanocubes with a side length of about 250 nm were synthesized by a modified method simlar to what has been reported in the literature[28]. The details can be found in supporting information[29]. The nanocubes were supported by an indium tin oxide (ITO) coated glass substrate. The experiments were performed using a commercial PEEM instrument (FOCUS IS-PEEM) together with a broadband few-cycle Ti:Sapphire laser oscillator (VENTEON Pulse-One), delivering pulses with a duration down to 5.5 fs with 1.55 eV central energy (800 nm central wavelength), 0.8 eV bandwidth, and 250 pJ pulse energy at

a repetition rate of 80 MHz. The laser pulse characteristics were monitored in a separate arm of the optical setup. The sample was illuminated at a 65 degree angle to the substrate normal, as seen in the schematic of Fig. 1a. The polarization could be adjusted using a broadband half-wave plate, and measurements were performed by continuously rotating the polarization in steps of 10 degrees. The nanocubes were imaged in the PEEM using two different light sources. A Hg discharge lamp provided topographic and work function contrast through 1-photon photoemission and was used to locate the nanocubes. The broadband laser pulses had a central photon energy of 1.55 eV, which is below half the work function of Ag(100) ($\sim$4.2 eV[30]), meaning that the absorption of at least 3 photons was required for each emitted electron. This nonlinear photoemission makes the image contrast sensitive to regions of enhanced electromagnetic fields, thus providing images of the enhanced near-field. The same nanocubes studied in the PEEM could afterwards be identified in a scanning electron microscope (SEM, Fig. 1b–c). We performed full polarization scans of 8 different cubes with random orientations with respect to the laser plane of incidence. As illustrative examples, we focus our analysis on the two nanocubes shown in Fig. 1b–c, one with its faces aligned with the plane of incidence, and one rotated by approximately 45 degrees. The FDTD simulations were performed using the commercial software FDTD Solutions from Lumerical. In the simulations, the dielectric function of Ag was fitted to literature data[31] and the nanocubes were lying on a fused silica substrate. The ITO layer was for simplicity not modeled. The corners of the cube were also kept sharp, as the radius of curvature of the cube corners has been shown to have minor qualitative effects on the optical response as long as it is much smaller than the side length[3,16]. The pulsed plane wave excitation was set to have a bandwidth matching that of the experimental laser pulses.

In order to compare FDTD simulations with experiments, we first confirmed the expected 3-photon photoemission process by measuring the photoemission intensity as a function of incident laser power. For a 3-photon process, we assumed that the photoemission yield originating from a point $\vec{r}$ of the sample surface can be calculated as[23] $Y(\vec{r}) \propto \int E_z(\vec{r},t)^6 \, \mathrm{d}t$, where E_z is the component along the surface normal of the near-field linearly induced by the short pulse excitation. Only photoelectrons originating from the top face of the cube were considered in modeling the PEEM images, because any electrons emitted from the sides of the nanocube would effectively have a high starting angle and therefore be blocked by the low-pass filtering contrast aperture of the PEEM[32]. Using FDTD, we calculated

the near field at the top face for both p- and s-polarized excitation (s-polarization means that the electric field is in the plane of the sample, as seen in the schematic of Fig. 1a). The electric field distribution was further calculated for an arbitrary polarization by making a linear combination of the simulated near-field induced by p- and s-polarized excitation, i.e. $\vec{E}(\vec{r},t,\theta) = \vec{E}_p(\vec{r},t)\cos\theta - \vec{E}_s(\vec{r},t)\sin\theta$. In this expression, $\vec{E}_p$ and $\vec{E}_s$ are the local electric fields when the cube is excited by p- and s-polarized light, respectively, and θ is the polarization angle as defined in Fig. 1a. The corresponding photoemission yield was eventually convolved by a Gaussian filter to account for the finite resolution of the PEEM. The simulated image intensity I for a polarization angle θ was thus calculated as:

$$I(\vec{r},\theta) = \int \left(E_{z,p}(\vec{r},t)\cos\theta - E_{z,s}(\vec{r},t)\sin\theta\right)^6 \mathrm{d}t \otimes \exp\left(-|\vec{r}|^2/2\sigma^2\right), \quad (1)$$

where σ is the standard deviation of the Gaussian filter and was set to 25 nm in our case.

Fig. 2 shows the experimental (a–d, i–l) multiphoton PEEM images for 4 different polarizations and for the two example cubes. For each polarization, the multiphoton photoemission is seen to be concentrated at the corners of the cubes, as opposed to the sides or the central part of the top face. Intensity localization is switched between different corners depending on the polarization of the incoming light, in accordance with both previous calculations[3,16] and experiments[17,18]. For both cubes, the photoemission is concentrated at the corners farther away from the excitation source, similar to what has been observed in studies of other metal nanostructures and attributed to a retardation effect[33,34]. As a result, the intensity can be selectively localized to three different corners (corners 1 through 3, as labelled in Fig. 1b) for the rotated cube (Fig. 2a–d) and two different corners (corners 1 and 2, Fig. 1c) for the cube aligned with the plane of incidence (Fig. 2i–l). For both cubes, photoemission from corners 1 and 2 is cancelled for a polarization close to p (Fig. 2a,i), however, the photoemission is seen to be simultaneously maximized for corner 3 for the rotated cube (Fig. 2a). On the contrary, the signal is evenly concentrated to both corners 1 and 2 for polarizations close to s (Fig. 2c,k). For both cubes it is possible to achieve maximum intensity at corners 1 and 2 separately by using intermediate polarizations between s and p. The photoemission can then be almost completely concentrated to one single corner within the experimental signal-to-noise ratio. Therefore, the on/off ratio between the photoemis-

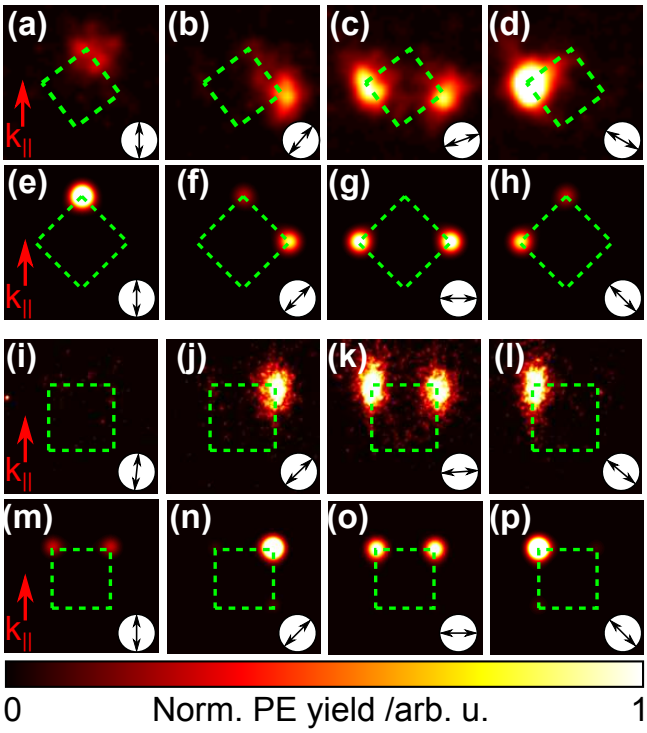

FIG. 2. (a–d) Experimental and (e–h) simulated multiphoton PEEM images of the nanocube shown in Fig. 1(b), for different polarizations of the incoming light. (i–l) Experimental and (m–p) simulated multiphoton PEEM images of the nanocube shown in Fig. 1(c) for different polarizations. All images are 500 × 500 nm^2 and the light is incident from the bottom. The polarizations are indicated with arrows depicting the electric field as seen in the direction of propagation (the angle θ as defined in Fig. 1a is increasing to the right). The green dashed lines represent the positions of the nanocubes in the images.

sion yield from the two different corners is difficult to determine because of the minimum signal being comparable to the noise floor. However, we estimate a lower limit of 50 for the on/off ratio between the two different corners by integrating the photoemission signal from each corner separately. The simulated images, obtained from FDTD simulations followed by Eq. 1, are shown for comparison in Fig. 2e–h and Fig. 2m–p. The simulated PEEM images are in excellent agreement with experiment. For the rotated cube, there is a small (up to $\sim 15°$) discrepancy in the exact polarization angles achieving the optimum concentration of the near-field into a specific single corner of the top face. Similarly to the cube aligned with the plane of incidence, this optimum concentration is achieved theoretically for $\theta = \pi/4$ (corner 2) and $\theta = 3\pi/4$ (corner 1). We attribute this discrepancy to the cube in the exper-

iment not being rotated by exactly 45 degrees, thus introducing some asymmetry. However, all features of the experimental images can be qualitatively reproduced in the simulations.

Contrary to previous works[3,16–18], the experiments were not performed at normal incidence. In addition, the nanocubes were larger than the typical sizes usually considered[3,9–19]. In order to connect the observed near-field localization to the optical properties of the nanocubes, we therefore performed additional FDTD simulations, with the rotated cube (seen in Fig. 1b) as example. Fig. 3a shows field enhancement spectra calculated at the four corners after excitation by time harmonic excitations of varying frequencies, both for p (a) and s (b) polarizations. The spectral features are in general broad due to the large size enabling a high radiative damping. For p polarization, the highest field enhancements are achieved at corner 3, with two resonances falling within our laser spectral bandwidth (marked as a red shaded area). Note, however, that the field enhancement is always between 5 and 7 across the laser spectral range. For s polarization, field enhancement is only obtained at corners 1 and 2, with only one resonance occuring in the laser bandwidth. Fig. 3c–e show the surface charge distributions associated with each resonance, calculated for p-polarization (3c–d) and s-polarization (3e). The charge distributions are not symmetric with respect to the center of the cube, because of the symmetry-breaking substrate and grazing incidence geometry leading to the resonances not reflecting pure single eigenmodes of the cube[13]. Nevertheless, the two p resonances are both associated with surface charge distributions symmetric with respect to the plane of incidence, while the s resonance is associated with a surface charge distribution antisymmetric with respect to the plane of incidence.

The experimentally demonstrated control of the near-field localization can be further understood in an intuitive picture of linear combinations of field distributions excited by s- and p-polarized light. The rotated cube is again considered as an example, but the general principle holds regardless of orientation. Fig. 4a–b show the local electric field as a function of time at the corners 1 and 2 for excitation by s- and p-polarized light, as extracted from the FDTD simulations. In accordance with Fig. 3, the fields at the two corners oscillate in phase for p polarization (green curves), and out of phase for s-polarization. If the polarization is tuned to $\theta = 3\pi/4$, the total near-field is $\vec{E}_{3\pi/4} = 1/\sqrt{2}\left(\vec{E}_p + \vec{E}_s\right)$, and the z-components of the electric fields add constructively in corner 1 and destructively in corner 2. Using a schematic illustration based on the charge distributions shown in Fig. 3, this linear combination is visualized in the drawings of Fig. 4c–e, illustrating regions of

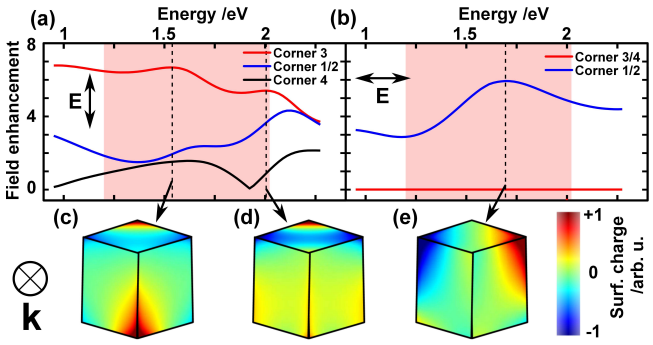

FIG. 3. (a–b) Field enhancement spectra calculated at the four corners of the rotated cube for both p (a) and s (b) polarizations. The red shaded area corresponds to the experimental laser bandwidth. (c–e) Surface charge distributions calculated at the resonances indicated by the black dotted lines in (a–b).

enhanced fields on the top face. A similar sketch corresponding to a polarization of $\theta = \pi/4$, which results in an enhanced field at corner 2 instead of 1 due to the sign change of the s-polarized component, is shown in Fig. 4f–h. While these pictures do not quantitatively reflect the time-integrated near field giving rise to the simulated images of Fig. 2, they do provide qualitative insight into near-field localization to specific corners. In both Fig. 4e and h, the field is mostly concentrated to a single corner of the top face of the cube. Turning the polarization by 90 degrees concentrates the near-field to the opposite corner. The highest field concentration to a single corner is found to be when the electric field vector of the exciting light is close to being aligned with the body diagonal of the cube. The same conclusion holds irrespective of the angle of the cube relative to the plane of incidence.

In summary, we demonstrate the subwavelength imaging and spatial control of localized near-fields within individual silver nanocubes. Through multiphoton PEEM combined with broadband, few-cycle laser pulses, we image the nonlinear photoemission from individual corners of nanocubes with various orientations with respect to the plane of incidence. We show how we can concentrate the photoemission to single corners of the cubes by tuning the polarization of the excitation light. The results are reproduced using finite-difference time-domain simulations showing excellent agreement with experiments. The mechanism behind the polarization switching only results from the geometry of the object, and could thus be extended to longer laser pulses[24,25]. Our findings thus generally establish nanocubes as an efficient as well as simple structure to locally concentrate electromagnetic energy from laser

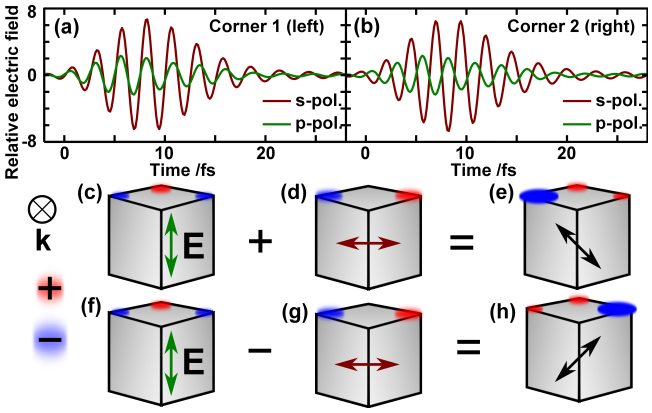

FIG. 4. Schematic visualization of the controlled near-field localization. (a–b) Normal component of the electric field in two opposite corners on the top face, calculated by FDTD for p- and s-polarization. (c–d) Schematic visualizations of the concentrated near-fields on the top face for p- and s-polarization, respectively. The cartoon 3D cubes are viewed from the direction of the incoming light, i.e. at grazing incidence. (e) Schematic of the sum of (c) and (d), corresponding to a polarization angle $\theta = 3\pi/4$. In analogy to (a–b), the electric fields add constructively at corner 1 (left) and destructively at corner 2 (right). (f–h) Same as (c–e), but with a negative sign of the s-polarized component, i.e. corresponding to a polarization angle $\theta = \pi/4$. **k** represents the propagation direction of the incoming radiation, and the polarization directions are labeled with arrows.

pulses in a deterministic manner. The active control of near-field localization in nanoscale objects opens up for applications within areas such as sensing, spectroscopy, and plasmonic devices.

ACKNOWLEDGEMENT

We acknowledge Hong Wei for nanoparticle synthesis. This work was supported by the Swedish Research Council (VR), the Swedish Foundation for Strategic Research (SSF), the Crafoord Foundation, the Knut and Alice Wallenberg Foundation, and the European Research Council (ERC) (startup grant ElectronOpera and advanced grant PALP).

REFERENCES

[1]J. N. Anker, W. P. Hall, O. Lyandres, N. C. Shah, J. Zhao, and R. P. Van Duyne, Nat Mater **7**, 442 (2008).

[2]J. Wessel, J. Opt. Soc. Am. B **2**, 1538 (1985).

[3]J. M. McLellan, Z.-Y. Li, A. R. Siekkinen, and Y. Xia, Nano Letters **7**, 1013 (2007), pMID: 17375965, http://dx.doi.org/10.1021/nl070157q.

[4]S. A. Maier, M. L. Brongersma, P. G. Kik, S. Meltzer, A. A. G. Requicha, and H. A. Atwater, Advanced Materials **13**, 1501 (2001).

[5]M. I. Stockman, S. V. Faleev, and D. J. Bergman, Phys. Rev. Lett. **88**, 067402 (2002).

[6]T. Brixner, F. J. García de Abajo, J. Schneider, and W. Pfeiffer, Phys. Rev. Lett. **95**, 093901 (2005).

[7]H. Wei, Z. Li, X. Tian, Z. Wang, F. Cong, N. Liu, S. Zhang, P. Nordlander, N. J. Halas, and H. Xu, Nano Letters **11**, 471 (2011), pMID: 21182282, http://dx.doi.org/10.1021/nl103228b.

[8]C. Rewitz, G. Razinskas, P. Geisler, E. Krauss, S. Goetz, M. Pawłowska, B. Hecht, and T. Brixner, Phys. Rev. Applied **1**, 014007 (2014).

[9]Y. Xia and N. J. Halas, MRS Bulletin **30**, 338 (2005).

[10]L. J. Sherry, S.-H. Chang, G. C. Schatz, R. P. Van Duyne, B. J. Wiley, and Y. Xia, Nano Letters **5**, 2034 (2005), pMID: 16218733, http://dx.doi.org/10.1021/nl0515753.

[11]F. Zhou, Z.-Y. Li, Y. Liu, and Y. Xia, The Journal of Physical Chemistry C **112**, 20233 (2008), http://dx.doi.org/10.1021/jp807075f.

[12]E. Ringe, J. M. McMahon, K. Sohn, C. Cobley, Y. Xia, J. Huang, G. C. Schatz, L. D. Marks, and R. P. Van Duyne, The Journal of Physical Chemistry C **114**, 12511 (2010), http://dx.doi.org/10.1021/jp104366r.

[13]S. Zhang, K. Bao, N. J. Halas, H. Xu, and P. Nordlander, Nano Letters **11**, 1657 (2011), pMID: 21410217, http://dx.doi.org/10.1021/nl200135r.

[14]P. R. Edwards, D. Sleith, A. W. Wark, and R. W. Martin, The Journal of Physical Chemistry C **115**, 14031 (2011), pMID: 23710265, http://dx.doi.org/10.1021/jp202083p.

[15]S. Mazzucco, N. Geuquet, J. Ye, O. Stphan, W. Van Roy, P. Van Dorpe, L. Henrard, and M. Kociak, Nano Letters **12**, 1288 (2012), pMID: 22263724, http://dx.doi.org/10.1021/nl2037672.

[16]A. Grubisic, E. Ringe, C. M. Cobley, Y. Xia, L. D. Marks, R. P. Van Duyne, and D. J. Nesbitt, Nano Letters **12**, 4823 (2012), pMID: 22845792, http://dx.doi.org/10.1021/nl302271u.

[17]M. Haggui, M. Dridi, J. Plain, S. Marguet, H. Perez, G. C. Schatz, G. P. Wiederrecht, S. K. Gray, and R. Bachelot, ACS Nano **6**, 1299 (2012), pMID: 22280022, http://dx.doi.org/10.1021/nn2040389.

[18]C. Deeb, X. Zhou, R. Miller, S. K. Gray, S. Marguet, J. Plain, G. P. Wiederrecht, and R. Bachelot, The Journal of Physical Chemistry C **116**, 24734 (2012), http://dx.doi.org/10.1021/jp304647e.

[19]O. Nicoletti, F. de la Pena, R. K. Leary, D. J. Holland, C. Ducati, and P. A. Midgley, Nature **502**, 80 (2013).

[20]V. Iberi, N. W. Bigelow, N. Mirsaleh-Kohan, S. Griffin, J. Philip D. Simmons, B. S. Guiton, D. J. Masiello, and J. P. Camden, The Journal of Physical Chemistry C **118**, 10254 (2014), http://dx.doi.org/10.1021/jp412778y.

[21]Y. Sun and Y. Xia, Science **298**, 2176 (2002), http://www.sciencemag.org/content/298/5601/2176.full.pdf

[22]M. Cinchetti, A. Gloskovskii, S. A. Nepjiko, G. Schönhense, H. Rochholz, and M. Kreiter, Phys. Rev. Lett. **95**, 047601 (2005).

[23]M. Aeschlimann, M. Bauer, D. Bayer, T. Brixner, F. J. Garcia de Abajo, W. Pfeiffer, M. Rohmer, C. Spindler, and F. Steeb, Nature **446**, 301 (2007).

[24]R. C. Word, J. Fitzgerald, and R. Könenkamp, Applied Physics Letters **99**, 041106 (2011).

[25]C. Hrelescu, T. K. Sau, A. L. Rogach, F. Jckel, G. Laurent, L. Douillard, and F. Charra, Nano Letters **11**, 402 (2011), pMID: 21244014, http://dx.doi.org/10.1021/nl103007m.

[26]E. Mårsell, A. Losquin, R. Svärd, M. Miranda, C. Guo, A. Harth, E. Lorek, J. Mauritsson, C. L. Arnold, H. Xu, A. L'Huillier, and A. Mikkelsen, Nano Letters **15**, 6601 (2015), pMID: 26375959, http://dx.doi.org/10.1021/acs.nanolett.5b02363.

[27]H. A. Atwater and A. Polman, Nat Mater **9**, 205 (2010).

[28]A. R. Siekkinen, J. M. McLellan, J. Chen, and Y. Xia, Chemical Physics Letters **432**, 491 (2006).

[29]See supplementary material at [URL will be inserted by AIP] for details on the nanocube synthesis.

[30]M. Chelvayohan and C. H. B. Mee, Journal of Physics C: Solid State Physics **15**, 2305 (1982).

[31]E. D. Palik, *Handbook of Optical Constants of Solids* (Academic, 1985).

[32]M. Lavayssière, M. Escher, O. Renault, D. Mariolle, and N. Barrett, Journal of Electron Spectroscopy and Related Phenomena **186**, 30 (2013).

[33]P. Melchior, D. Bayer, C. Schneider, A. Fischer, M. Rohmer, W. Pfeiffer, and M. Aeschlimann, Phys. Rev. B **83**, 235407 (2011).

[34]Q. Sun, K. Ueno, H. Yu, A. Kubo, Y. Matsuo, and H. Misawa, Light Sci Appl **2**, e118 (2013).